LUND UNIVERSITY
Faculty of Science

Motion of a Gaussian Through a 2D Dilute BEC Droplet

Zhanna Kuhrij

Thesis submitted for the degree of Bachelor of Science
Project duration: 2 months (15 hp)

Supervised by Stephanie M. Reimann and co-supervised by Mikael Nilsson Tengstrand

Department of Physics
Division of Mathematical Physics
May 2020

Acknowledgements

I would like to sincerely thank my supervisor Stephanie M. Reimann and my co-supervisor Mikael Nilsson Tengstrand for their continuous dedication, enthusiasm and support while writing my thesis. I would also like to thank them for letting me be a part of the research group. Further, I would like to thank my co-supervisor Mikael Nilsson Tengstrand for letting me use his propagation in imaginary time code. I would also like to thank my co-supervisor Mikael Nilsson Tengstrand and Philip Stürmer for letting me use their code to plot the densities and phases of the dilute BEC droplets. Then, I would like to thank my office companion David Boholm for being so kind and helpful, and also the rest of the research group for being so inclusive. I would also like to thank my boyfriend Emmanuel D Costa for making every day better, and my parents for always looking after and supporting me. Finally, I would like to thank all my friends and last but not least my cat Puma and dog Alva for their great companionship.

Abstract

In the last decades, Bose-Einstein Condensates (BECs) have been a research topic of great interest. In 2015, a new type of liquid was found - dilute self-bound BEC droplets that have orders of magnitude lower density than air. These droplets are not predicted by classical van der Waals theory, but are stabilised by quantum fluctuations. In this bachelor thesis, these droplets were numerically studied when colliding with a Gaussian obstacle in two-dimensions. This is interesting because below a certain velocity, dilute BECs can behave like superfluids. This is called Landau's criterion. Several droplet velocities and Gaussian widths were tested with special focus on two cases: one where the droplet starts outside the Gaussian and one where the droplet starts with the Gaussian inside of it. The droplet was then propagated until the Gaussian was approximately at the centre of the droplet. In none of the collisions simulated, laminar- attached vortices- or vortex street flow patterns were observed. These are flow patterns one can see in similar classical examples and/or with trapped dilute BECs. However, it appeared that in all the cases the droplet did not fully behave like a superfluid. It might have been quantum fluctuations that created a drag force. Further, a large deformation of the droplet could be seen when the droplet started outside a broad Gaussian. This is believed to have been caused by the Gaussian piercing the surface of the droplet. Finally, suggestions for future research are given at the end of this thesis.

List of Abbreviations and Acronyms

BEC	Bose-Einstein Condensate
GPe	Gross-Pitaevskii equation
LHY correction	Lee-Huang-Yang correction
2D	Two-Dimensional
3D	Three-Dimensional

Contents

Chapter 1

Introduction

Unlike fermions, more than one boson can be in the same quantum state at the same time [1]. If many bosons in a system occupy the ground state, it is called a Bose-Einstein Condensate (BEC) [2]. BECs were first predicted theoretically in the 1920s by S. N. Bose and A. Einstein. In 1995, atomic dilute BECs were first created in a lab [3]. The experimental achievement earned a Nobel prize and BECs remain a relevant and interesting research topic until today [4].

Weakly-interacting dilute BECs can be described by Bogoliubov theory [3]. The mean-field approximation can also be applied for dilute BECs [2]. In the mean-field approximation, all interactions between individual particles in a system are approximated by an average potential [5]. Bogoliubov theory together with the mean-field approximation give the Gross-Pitaevskii equation (GPe), which is a non-linear Shrödinger equation that models dilute BECs [2, 3]. The GPe is often solved numerically by using propagation in imaginary time [6, 7].

In 2015, dilute self-bound BEC droplets were predicted theoretically by D. S. Petrov [8, 9]. Since then, they have also been found experimentally [10, 11, 12]. The densities of these BECs are orders of magnitude lower than the density of air, but the BECs still form liquid droplets. This is opposed to what classical van der Waals theory predicts, which is a gas. What makes these BECs self-bound is quantum fluctuations. If the mean-field term in the GPe becomes small enough, beyond mean-field corrections become important. The first correction is the Lee-Huang-Yang correction (LHY correction) [13] and is based on quantum fluctuations due to Heisenberg's uncertainty principle. A way to make the mean-field term small is to have a BEC consisting of two types of bosons, where the intra-species interaction is repulsive, the inter-species interaction is attractive and the two interactions are of similar magnitude [9].

Dilute BECs behave differently compared to classical fluids. Below a certain velocity, they can behave like superfluids [2]. A superfluid can flow past an obstacle without friction [14]. Despite this, there are some similarities between flow patterns of classical fluids and flow patterns of two-dimensional 2D dilute BECs. A common example in classical fluid dynamics is flow past a cylinder [15]. This is because cylinders are simple geometric objects

and already give complicated flow patterns [16]. Similar studies have been performed with 2D or quasi-2D dilute BECs using Gaussians [15]. However, no such studies have yet been reported for dilute BEC droplets.

The aim of this thesis is to numerically simulate what happens when a 2D dilute BEC droplet, consisting of two types of bosons, collides with a Gaussian potential. Two cases were especially considered: one where the Gaussian starts outside the droplet, and one where the Gaussian starts inside the droplet, relatively far away from the droplets edge. In the second case, the Gaussian starts relatively far away from the surface of the droplet in order to neglect surface effects as much as possible. The droplet is then given a velocity and studied when the Gaussian is approximately in the centre of it, if it did not deform too much, see figure 1.1. Different velocities and Gaussian widths are tested. The reason a 2D simulation is done instead of a three-dimensional (3D) one, is that the 3D case could be more complicated than the 2D case. One more dimension might give more complex phenomena. It is therefore better to consider the 2D case first. Numerical simulations in 3D also require more computing power.

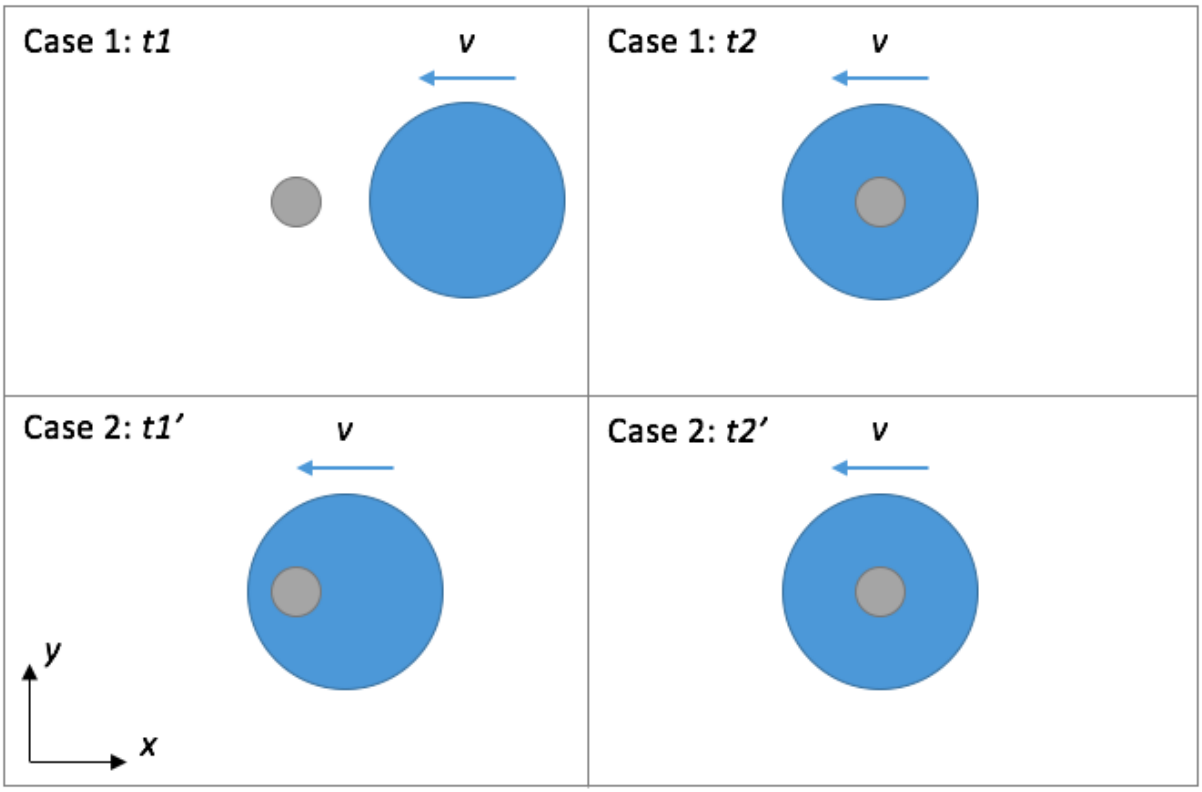

Figure 1.1: The two different cases considered in detail in the thesis. The grey disk symbolises the Gaussian and the blue disk the droplet. In one case, the Gaussian started outside the droplet at time $t_1 = 0$ and in the other case inside at $t_1' = 0$. The droplet was then given a velocity v to the left in the x-direction. Finally, it was studied at t_2 and t_2': when the Gaussian was approximately in the middle of the droplet, if it did not deform too much.

Chapter 2

Theory

2.1 Dilute BECs

An ideal BEC is be made out of non-interacting bosons. This was the case considered in the 1920s. At 0 K, all bosons in such a BEC will be in the ground state [3]. However, for interacting bosons, it is not obvious beforehand if all will be in the ground state at 0 K. Now we know that many of the bosons in such a BEC will be in the ground state at absolute zero [4].

In order to model BECs, approximations are often made [2, 3]. Dilute and weakly-interacting BECs can be described by Bogoliubov theory. In these BECs, the range of the interatomic potential is much smaller than the average distance between the bosons. Also, in order to form a BEC in the first place, the temperature must be lower than a critical temperature. These two conditions lead to the requirement that

$$r_0 \ll \lambda_{dB}. \tag{2.1}$$

In equation 2.1, r_0 is the range of the interatomic potential and λ_{dB} is the thermal de Broglie wave length of the bosons [1, 3]. Equation 2.1 thus implies that the bosons cannot resolve the interatomic potential, see figure 2.1. This means that the interaction potential between the bosons often can be simplified according to [9]

$$V_{int}(r) = g\delta(r). \tag{2.2}$$

In equation 2.2, r is the distance between two bosons and g is a coupling constant proportional to the s-wave scattering length a [3, 9]. The s-wave scattering length is used with low-energy collisions [3]. The definition of scattering length is not very intuitive and can be found in [2].

2.2 The Mean-Field Approximation and GPe

To solve the Schrödinger equation for a system of non-interacting particles is relatively easy. The wave function of such a system can be written as a symmetrized or anti-symmetrized product of the single-particle wave functions. However, if the particles are interacting, it is

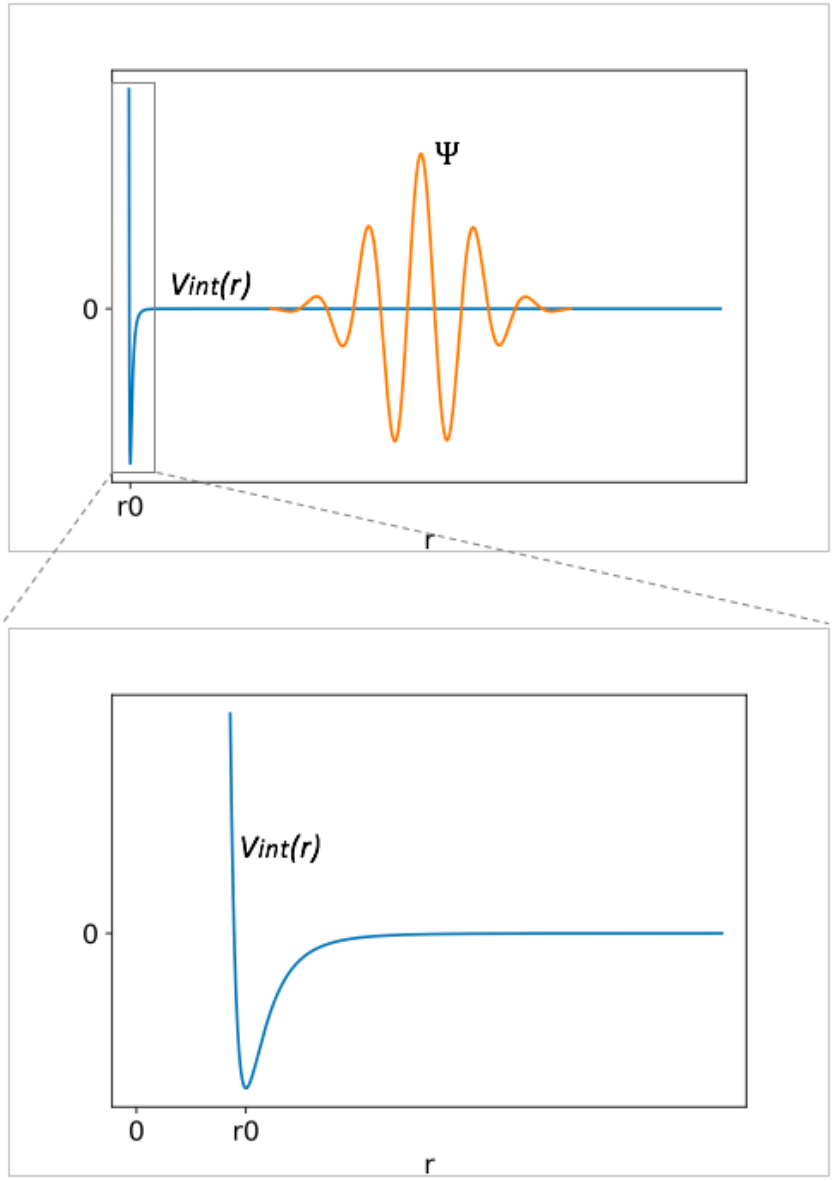

Figure 2.1: The wavelength of the bosons in a dilute BEC is too large in order to resolve the interatomic potential $V_{int}(r)$. This means that the inter atomic potential often can be simplified according to equation 2.2. The wave function of the bosons is denoted Ψ [9]. The figure is based on a figure in [9].

harder or impossible [5]. Therefore, approximations are often made [2, 5]. The mean-field approximation is one of these [5].

The exact Hamiltonian of a system of non-relativistic pairwise interacting particles with an external potential is

$$\hat{H} = \sum_{i=1}^{N} (\hat{t}_i + \hat{u}_i) + \frac{1}{2} \sum_{\substack{i,j=1 \\ i \neq j}}^{N} \hat{v}_{ij}, \tag{2.3}$$

where N is the number of particles in the system, i and j denote the different particles, $\hat{t}$ denotes the kinetic energy, $\hat{u}$ the external potential and $\hat{v}_{ij}$ the interaction potential between particles i and j [5, 17]. The coefficient $\frac{1}{2}$ takes care of double counting. In the mean-field approximation, the wave function of a system of weakly interacting particles is assumed to be a Slater determinant or permanent of the single-particle wave functions, just like in the non-interacting case. The expectation value of the exact Hamiltonian of the system is then minimised according to this ansatz, using Ritz' variational theorem. This gives a new "effective" Hamiltonian [5].

As mentioned before, for a dilute BEC, the interaction between particles can also often be replaced with the potential in equation 2.2 [1, 3]. Another approximation that can be made, despite that the bosons are weakly interacting, is they all are in the ground state [3]. This gives the expression

$$E(\Psi_0) = \int \left(\frac{\hbar^2}{2m} |\vec{\nabla} \Psi_0(\vec{r})|^2 + V_{ext}(\vec{r}) |\Psi_0(\vec{r})|^2 + \frac{1}{2} g |\Psi_0(\vec{r})|^4 \right) d\vec{r}, \tag{2.4}$$

which is minimised together with a normalisation constraint. Note that in equation 2.4, E is the energy of the system, $\Psi_0(\vec{r})$ is the ground-state of the BEC wave function, m is the mass of a single boson in the BEC and $V_{ext}(\vec{r})$ is the external potential. This finally gives

$$\mu \Psi_0(\vec{r}) = \left(-\frac{\hbar^2 \nabla^2}{2m} + V_{ext}(\vec{r}) + g |\Psi_0(\vec{r})|^2 \right) \Psi_0(\vec{r}). \tag{2.5}$$

Equation 2.5 is called the Gross-Pitaveskii equation (GPe) and is used to model dilute BECs. In equation 2.5, μ is the chemical potential. So, by using the mean-field approximation, all the interactions between individual bosons in a dilute BEC are simplified by an average potential experienced by all bosons [2].

A solution to the GPe can always be written as

$$\Psi(\vec{r}, t) = \sqrt{n(\vec{r}, t)} e^{iS(\vec{r}, t)}. \tag{2.6}$$

In equation 2.6, $\vec{r}$ contains the spacial coordinates, which in 2D can be written (x, y), $n(\vec{r}, t)$ is the density of the wave function and $S(\vec{r}, t)$ is called the phase of the wave function [4].

If a 2D dilute BEC consists of two types of bosons with the same intra-species interaction and mass, the GPe can be written as

$$\mu \Psi_0(\vec{r}) = \left(-\frac{\hbar^2 \nabla^2}{2m} + V_{ext}(\vec{r}) + \frac{\hbar^2 8\pi}{m \ln^2(a_{12}/a_{11/22})} \ln \left(\frac{|\Psi_0(\vec{r})|^2}{\sqrt{e} n_0} \right) |\Psi_0(\vec{r})|^2 \right) \Psi_0(\vec{r}). \tag{2.7}$$

for the system. In equation 2.7, $a_{11/22}$ is the 2D intra species s-wave scattering length, a_{12} the 2D inter species s-wave scattering length, e is the natural number and n_0, which is the equilibrium density of each type of boson, is given by

$$n_0 = \frac{e^{-2\gamma-(3/2)} \ln(a_{12}/a_{11/22})}{2\pi a_{12} a_{11/22}}, \tag{2.8}$$

where $\gamma = 0.577$ is the Euler-Mascheroni constant. The third term in equation 2.7 contains both the boson interactions and quantum fluctuations, which will be described in section 2.3 [18]. If $n = |\Psi_0(\vec{r})|^2$, which is the density of the bosons, one can also see that the third term has a minimum, since $\ln(n)n$ does [2]. This suggests that there should be a bound state with a minimum energy without an external potential. This is not the case in equation 2.5.

Even though the GPe is a simplification of the exact Hamiltonian, it is a non-linear Schrödinger equation and is often solved numerically [4, 6, 7].

2.3 Dilute BEC Droplets

The difference between a gas and a liquid is relatively simple: a gas fills the whole space available to it, while a liquid does not necessarily. So, gases usually also have lower densities than liquids. According to classical van der Waals theory, a liquid is formed when the distance between the particles is small enough for them to feel an attractive force, which is balanced by a short-range repulsion, see $V_{int}(r)$ in figure 2.1 [9].

As mentioned before, the interatomic potential for a dilute BEC can be simplified according to equation 2.2. If g in that formula is positive, the particles in the BEC will repel each other. If on the other hand g is negative, the particles will attract each other. In the first case the BEC expands and in the second case the BEC collapses. Neither of these cases lead to a liquid dilute self-bound BEC droplet [9].

Dilute BEC droplets can form when the mean-field term in the GPe (the term furthest to the right in equation 2.5) becomes small enough for beyond mean-field corrections to become important. The first correction to the mean-field term is the LHY correction, which is based on zero-point quantum fluctuations. I.e., even if all the particles in the BEC would be in the ground state, particles can still momentarily "jump" to higher energy levels according to Heisenberg's uncertainty principle [9].

A way to make the mean-field term small is to make the magnitude of g small. This can be achieved by having two types of interactions of the same magnitude in a BEC: one repulsive and one attractive. If the BEC is made out of two different atomic species named 1 and 2, where the intra species potential is repulsive and the inter species potential is attractive, the net g-value becomes

$$\delta g = g_{11/22} - g_{12}. \tag{2.9}$$

(Note that here $g_{12} > 0$, i.e. the minus sign is explicit). In equation 2.9, the index 11/22 means intra species and the index 12 inter species. The two intra species interaction are thus the same and labeled $g_{11/22}$ [9].

The "strength" of the mean-field term is proportional to $\delta g \rho^2$ while the "strength" of the LHY correction is proportional to $g_{12}(g_{11/22})^{3/2}\rho^{5/2}$, where ρ is the density of the BEC. The LHY correction contributes with an effective repulsion. If then

$$g_{11/22} < g_{12} \tag{2.10}$$

δg becomes negative, with gives an attractive force. If $g_{11/22}$ and g_{12} are not individually small, the strength of the mean-field term and LHY correction can then be balanced by adjusting the density: a liquid dilute BEC droplet can be made. The densities of these BEC droplets are still very low and classical van der Waals theory does not predict a liquid state. It is a quantum mechanical effect [9].

To form a dilute BEC droplet, there must also be a certain number of particles in the BEC. This is because the surface tension also has some energy, which can turn the droplet into a gas. Note also that the densities of these droplets are not uniform, they decrease going outwards from the centre. Finally, these droplets only live for a short time (typically a few to tens of milliseconds) because of three body losses. Three body losses are when two atoms turn into a molecule and thus reduce the atom particle number: the droplet eventually breaks down. It is called three body losses because three atoms need to be part of the collision to conserve momentum and energy [9].

An example of two different atomic species that can be used to create a dilute BEC droplet is two different hyperfine states of potassium [19]. Instead of two atomic species, one can also have one type of atom with a large magnetic moment. The two different interactions are then the contact interaction between the atoms and the dipole-dipole interaction. The g-value can be tuned using Feshbach resonances [9]. In Feshbach resonances, the scattering length between two particles can be altered using an external magnetic field. This is possible because the energies of the different hyperfine states, which give the different scattering lengths, are dependent on for example the magnetic field [2].

The above discussion applies to 3D dilute BEC droplets. In the 2D case, the situation is somewhat different, but conceptually similar [8, 18].

2.4 Fluid Dynamics

A common example in classical fluid dynamics is flow past a cylinder [15]. The cylinder is long and thin in order to neglect edge/surface effects and is placed with its axis perpendicular to the flow [16]. The reason a cylinder is often used is because it has a relatively simple geometric shape and its flow patterns are already complicated [15, 16].

The flow patterns of a classical fluid flowing past a cylinder depend on the Reynolds number

$$\mathrm{Re} = \frac{\rho u_0 d}{\eta}. \tag{2.11}$$

In equation 2.11, ρ is the density of the fluid (which is approximated to be constant), u_0 is the magnitude of the velocity of the fluid far away from the cylinder, d is the diameter of the cylinder and η is the viscosity of the fluid [16]. Viscosity is the internal friction of a fluid [20]. If ρ, d and η are set, the flow patterns thus depend on u_0.

For $\mathrm{Re} \lessapprox 4$, the flow is laminar. The flow is then symmetric around the cylinder. For $4 \lessapprox \mathrm{Re} \lessapprox 40$, a wake is formed with two vortices attached to the back of the cylinder [16]. A wake is the flow behind a cylinder that is different from that in front [15, 16]. As the Reynolds number increases, the two vortices become bigger. At $40 \lessapprox \mathrm{Re} \lessapprox 100$, the flow is also affected much further away from the back of the cylinder. At $\mathrm{Re} \approx 100$, the so-called Kármán vortex street forms. The two vortices that were previously attached to the back of the cylinder are now shed of and reformed periodically, this is called vortex shedding. When the Reynolds number is further increased the flow eventually becomes turbulent. Turbulent means that there are irregular and rapid changes in the velocity of the fluid [16]. If wanted, a visualisation of most of the flow patterns discussed above can be found in figure 1 in [15].

Note that it does not matter whether the fluid or cylinder is moving, as long as it is at constant velocity. The cylinder can thus also be moved through a fluid at rest. u_0 in equation 2.11 is then the velocity of the cylinder. Further, the formation of a wake is due to an increasing drag on the cylinder. Drag is the force that the liquid exerts on the cylinder and it increases with viscosity as well as with velocity [16].

For dilute BECs, the situation is different compared to classical fluids. When dilute BECs of uniform density flow past a heavy obstacle below a certain velocity, they can behave like superfluids. This is called Landau's criterion. Note that it again does not matter whether the obstacle or BEC is moving, if they move at a constant velocity [2]. A superfluid can flow without friction, i.e. $\eta = 0$. Because the viscosity is zero, no Reynolds number can be defined [15]. Above the critical velocity, excitations start to occur in the BEC which leads to a drag force. The dilute BEC can now be described by the two-fluid model. In the two-fluid model, the BEC is said to be made out of two components: one superfluid component and one excited component behaving like a classical fluid [2]. For dilute BECs, the critical velocity is around the speed of sound [15].

One other important property of dilute BECs is the formation of quantised vortices. Quantised vortices means that the circulation C of the BEC velocity is quantised according to

$$C = \oint \vec{v} \cdot d\vec{l} = \frac{h}{m} l. \tag{2.12}$$

In equation 2.12, $\vec{v}$ is the velocity of the BEC, h is Planck's constant, m is the mass of

a single boson in the BEC and l is an integer [2]. Even though classical fluids can have vortices, they are not quantised. Therefore this might change the flow patterns of a dilute BEC compared to a classical fluid [15]. Quantised vortices have been experimentally found in dilute trapped BECs and theoretically predicted for dilute BEC droplets, despite their surface tension [21, 22, 23].

Finally, the velocity of a dilute BEC is given by

$$\vec{v} = \frac{\hbar}{m} \nabla S, \tag{2.13}$$

where m again is the mass of a single boson in the BEC and S is the phase of the BEC wave function [2]. This means that the velocity of the BEC may be deduced from a plot of the phase of the wave function.

Several studies have been performed on what happens when a 2D or quasi-2D dilute trapped BEC flows past a Gaussian obstacle, which is then similar to a cylinder [15]. In one of the studies, a laser was used as a Gaussian potential of different sizes, which was then moved through the trapped BEC [15, 24]. Beneath a critical velocity, the flow was laminar around the Gaussian. When the Landau criterion was broken, a wake was observed with a kind of vortex street. At even higher velocities, another type of vortex street was observed. Both of these two vortex streets had different patterns compared to the classical Kármán vortex street (but vortices were still shed from the back of the Gaussian periodically). If the velocity was further increased, the flow eventually became chaotic [15].

Chapter 3

Method

3.1 Propagation in Imaginary Time

As mentioned in the introduction, the GPe is a non-linear Schrödinger-like equation and often solved numerically [4, 6, 7]. Today, this is often done using propagation in imaginary time [6, 7].

The idea behind propagation in imaginary time is to use the evolution operator

$$\hat{T} = \exp(\frac{-it\hat{H}}{\hbar}) \tag{3.1}$$

to find the ground state of the Schrödinger equation. Note that in equation 3.1, t is real time and $\hat{H}$ is the Hamiltonian of the system. The operator can also be written as

$$\hat{T} = \exp(\frac{-\tau\hat{H}}{\hbar}) \tag{3.2}$$

where

$$\tau = it \tag{3.3}$$

is imaginary time [25].

The stationary wave function of a system can be written as a sum of basis functions corresponding to different energies

$$\Psi(\vec{r}, \tau = 0) = \Psi(\vec{r}, 0) = \sum_i c_i \phi_i(\vec{r}). \tag{3.4}$$

In equation 3.4, $\vec{r}$ are the spacial coordinates and c_i are coefficients. The time-dependent wave function is then given by acting with the evolution operator upon the stationary wave function, where the Hamiltonian in the evolution operator can be replaced with the different energies [25]

$$\Psi(\vec{r}, \tau) = \hat{T}\Psi(\vec{r}, 0) = \sum_i \exp(\frac{-\tau E_i}{\hbar}) c_i \phi_i(\vec{r}). \tag{3.5}$$

The Hamiltonian is a Hermitian operator, which means that its eigenvalues are real and positive. E_0 corresponds to the ground state energy and hence

$$E_0 < E_1 < E_2..., \tag{3.6}$$

assuming no degeneracy. In propagation in imaginary time, τ is propagated from zero towards infinity. The higher the energy, the faster the corresponding exponential in equation 3.5 will decay away, see figure 3.1 [25].

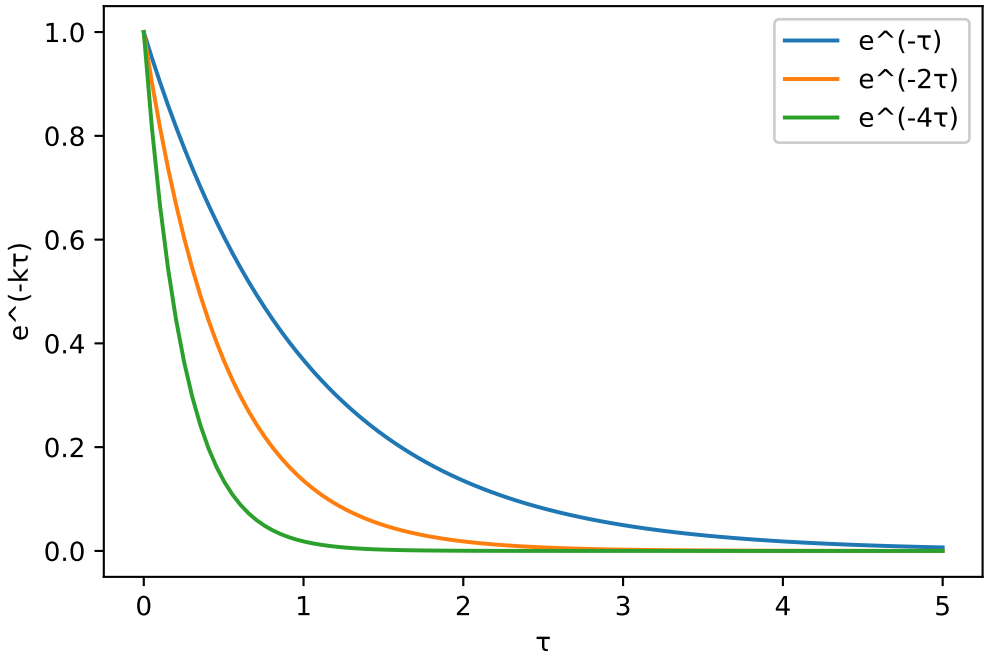

Figure 3.1: $\exp(-k\tau)$ decays faster, when τ is propagated from zero towards infinity, if k is larger. (The y-axis shows the value of the exponentials).

This means that the following equation gives the ground state Ψ_0 of the Schrödinger equation

$$\lim_{\tau\to\infty} \Psi(\vec{r},\tau) = \exp(\frac{-\tau E_0}{\hbar}) c_0\phi_0(\vec{r}) = \Psi_0. \tag{3.7}$$

This is regardless of what function $\Psi(\vec{r},0)$ one starts with [25].

However, on a computer, one cannot take infinitely many and small time-steps. Note also that the effective Hamiltonian of the GPe contains the wave function [2]. This means that the evolution operator also contains the wave function and therefore it needs to be "updated" at every time-step.

When solving the Schrödinger equation on a computer using propagation in imaginary time, splitting methods with Fourier transforms are also used. In these splitting methods,

the evolution operator is split into several factors containing the different parts of the Hamiltonian (or effective Hamiltonian for the GPe) [25]. This makes it faster for the computer to solve [26]. However, it introduces an error that is dependent on the time-step size [25].

The time-step size is chosen such that it does not give a to large error (one can approximate this). The propagation is finally stopped when the result has converged [7].

3.2 Dynamics of Dilute BEC Droplet

In this thesis, a dilute BEC droplet was first created in vacuum using propagation in imaginary time. Then, at real time $t = 0$, a Gaussian obstacle was introduced. At this point, the droplet was either positioned with the Gaussian outside of it or with the Gaussian inside of it, relatively far away from the surface, see figure 1.1. As mentioned before, in the second case, the Gaussian starts relatively far away from the surface of the droplet in order to neglect surface effects as much as possible.

An initial velocity was then given to the droplet by using equation 2.13. After this, the droplet was propagated in real time until the gaussian was approximately at the centre of it, if the droplet did not deform to much, see figure 1.1. Two different sizes of real time steps were tried in order to see if the dynamical results were converged: $\Delta\tilde{t} = 10^{-2}$ and $\Delta\tilde{t} = 10^{-3}$. See section 3.3 for unit conversions.

In this thesis, three different velocities of the droplet and three Gaussians with different widths are presented. Each combination of velocity and Gaussian width was tested starting with the Gaussian outside of the droplet and with the Gaussian inside. A Gaussian can be written

$$V(x, y) = A\exp\left(-\frac{(x - b_x)^2}{2c_x^2} + \frac{(y - b_y)^2}{2c_y^2}\right), \tag{3.8}$$

where A is the amplitude of the gaussian, b_x, b_y is where the Gaussian is centred in the (x, y)-plane and c_x and c_y are related to the width of the Gaussian in the x- and y-direction, respectively [27]. In this thesis

$$c_x = c_y = c \tag{3.9}$$

was always used.

Since the GPe only is valid when few excitations are present in a BEC, therefore to high velocities were not tested. Three-body losses were not included in the simulations, which is a good starting point. Note that all simulations were done in 2D. A grid of 512×512 points was used. The code was borrowed from [28]. One simulation took from below a minute to about five minutes depending on the time step size and number of time steps (different velocities required different times to get the droplet in the same position).

3.3 Scaling of the GPe

In order to make computations easier, the GPe was solved using dimensionless variables. In the results section, distances (c-value for Gaussian) and velocities will be given in the corresponding dimensionless units. The transformation of distance, time and velocity from dimensionless units to real ones are

$$x = \frac{\ln(a_{12}/a_{11/22})}{\sqrt{8\pi n_0 \sqrt{e}}}\tilde{x}, \tag{3.10}$$

$$t = \frac{m \ln^2(a_{12}/a_{11/22})}{8\pi\hbar n_0 \sqrt{e}}\tilde{t} \tag{3.11}$$

and

$$v = \frac{\hbar\sqrt{8\pi n_0 \sqrt{e}}}{m \ln(a_{12}/a_{11/22})}\tilde{v}. \tag{3.12}$$

In equations 3.10, 3.11 and 3.12, the tildes mark the dimensionless variables. x is distance, t is time and v is velocity. $a_{11/22}$ and a_{12} are the 2D intra and inter species s-wave scattering lengths, m is the mass of a single boson in the BEC, e is the natural number and n_0 is given in equation 2.8 [18].

Chapter 4

Results and Discussion

4.1 Gaussian Starting Outside the Droplet

When the Gaussian starts outside the dilute BEC droplet, see figure 1.1, one cannot directly compare the results with the classical fluid case considered in section 2.4 (a large body of classical fluid with a small obstacle, not a droplet) and the trapped BEC case. This is because those cases neglect boundary/surface effects, which clearly are present when the Gaussian pierces the surface of the droplet. However, the case in itself is still interesting and can also be compared with when the Gaussian starts inside the droplet. Landau's criterion is also not relevant for the same reason. But one can still see if the droplet behaves like a superfluid or not, without referring to it as Landau's criterion.

Figure 4.1 shows the density distribution of the droplet for different Gaussian widths and droplet velocities at time t_2 in figure 1.1. To recall, at t_2, the droplet is positioned with the Gaussian approximately in the centre of it, if the droplet did not deform too much. For comparison, figure 4.2 shows how the droplet looks at time t_2 with a dimensionless velocity $\tilde{v} = 0.4$ if no obstacle is present. The corresponding phase plot is also included in the figure, which shows a constant change in the phase as expected by equation 2.13 at a constant velocity. If another velocity would have been taken as example, only the phase plot would change according to equation 2.13. If the droplet would not have moved anymore, the phase plot would have showed a constant value, which according to equation 2.13 indeed gives zero velocity. The faster the velocity, the faster the phase changes. In all the plots of figure 4.1, a relative density scale is used. This means for example that dark red will always be the highest density in each plot, but it might not correspond to the same density value in each plot. The reason a relative density scale was used is to see small density variations within the droplet.

Note that for different velocities, t_2 is different. However, since no three-body losses were taken into account in the simulations, this is not a problem. For the time scales used, with no obstacle present, the density of the droplet looks the same with one velocity and t_2 as with half the velocity and double the t_2.

For all the plots in figure 4.1, the density distribution within the droplet looks different

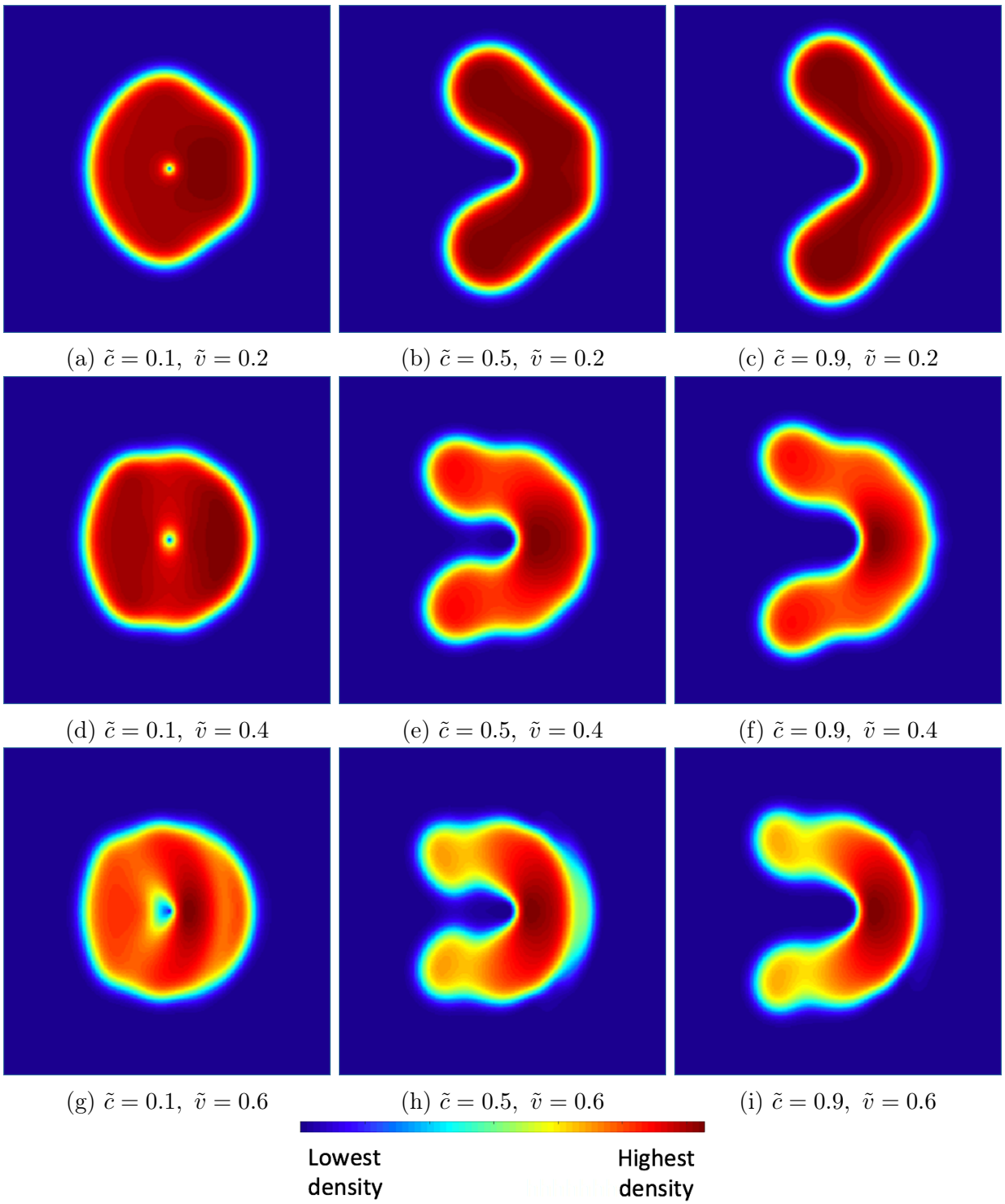

(a) $\tilde{c} = 0.1,\ \tilde{v} = 0.2$ (b) $\tilde{c} = 0.5,\ \tilde{v} = 0.2$ (c) $\tilde{c} = 0.9,\ \tilde{v} = 0.2$

(d) $\tilde{c} = 0.1,\ \tilde{v} = 0.4$ (e) $\tilde{c} = 0.5,\ \tilde{v} = 0.4$ (f) $\tilde{c} = 0.9,\ \tilde{v} = 0.4$

(g) $\tilde{c} = 0.1,\ \tilde{v} = 0.6$ (h) $\tilde{c} = 0.5,\ \tilde{v} = 0.6$ (i) $\tilde{c} = 0.9,\ \tilde{v} = 0.6$

Figure 4.1: Density distribution of the dilute BEC droplet when the Gaussian started outside the droplet, for different Gaussian widths and droplet velocities, at time t_2 in figure 1.1. The dimensionless Gaussian sizes $\tilde{c}$ and velocities $\tilde{v}$ are given in the figure. Note that for example dark red is the highest density in each plot, but that it might not correspond to the same density value in all of them. The Gaussians are not plotted in the figure, but are in the middle of each plot. They can in part indirectly be seen by the interaction with the droplet.

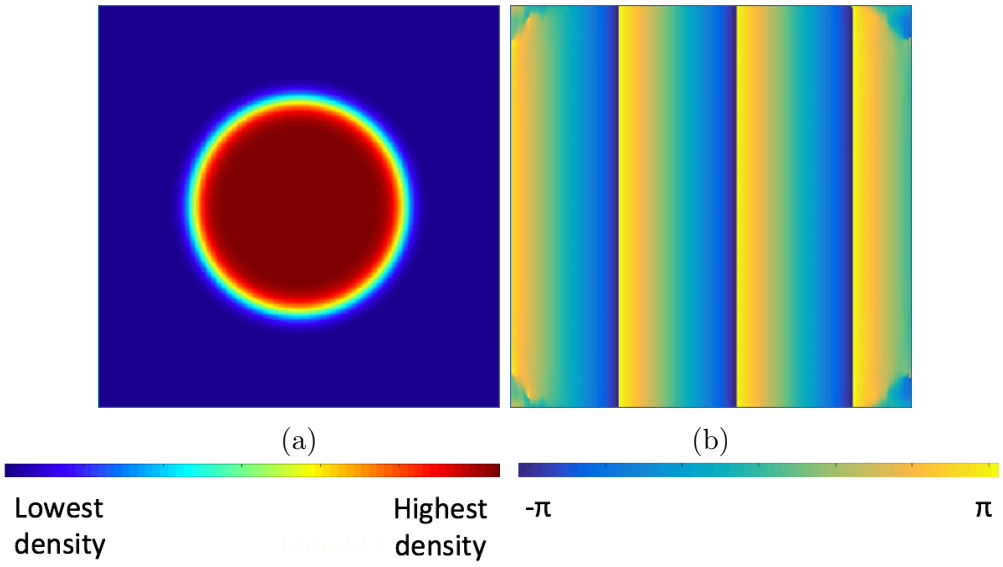

Figure 4.2: Density distribution (a) and phase (b) of a dilute BEC droplet at time t_2 (or t_2') in figure 1.1 with $\tilde{v} = 0.4$ if no obstacle is present. The density and phase plot have the same scale (in size).

from that in figure 4.2. This indicates that the velocities must have been affected either by the Gaussian piercing the droplet or by a drag force, which creates density variations within the droplet. However, when comparing to the case when the Gaussian starts inside the droplet (see next section), similar density variations are seen there without the Gaussian piercing the surface initially. So, it appears that the droplet no longer fully behaves like a superfluid. Besides this, the droplet has deformed much for all velocities for the two broader Gaussians: it has not fully recombined behind the Gaussian. However, in figures 4.1 (e) and (h), one can see that droplet is starting to recombine behind the Gaussian. The phase plots for figures 4.1 (e), (g) and (h) are shown in figure 4.3. In the corresponding density plots, there is a clear wake behind the Gaussian, but in neither of the phase plots there is an indication of vortices attached to the Gaussian, according to equation 2.13. There is also no indication of vortex streets, which would have be seen in the density plots as a row of density singularities. However, one can clearly see that the velocity is indeed disrupted, since the change in the phase no longer is constant in any of the plots.

Why the flow patterns look the way they do (when the droplet not behaves fully like a superfluid) in figure 4.1 is very hard to explain. As mentioned in the theory, even for a classical fluid and a cylinder it is hard to explain the reason for the flow patterns. However, what one can do is to search for for example vortices that are known to appear in flow patterns.

It might be quantum fluctuations that are responsible for the drag force [29].

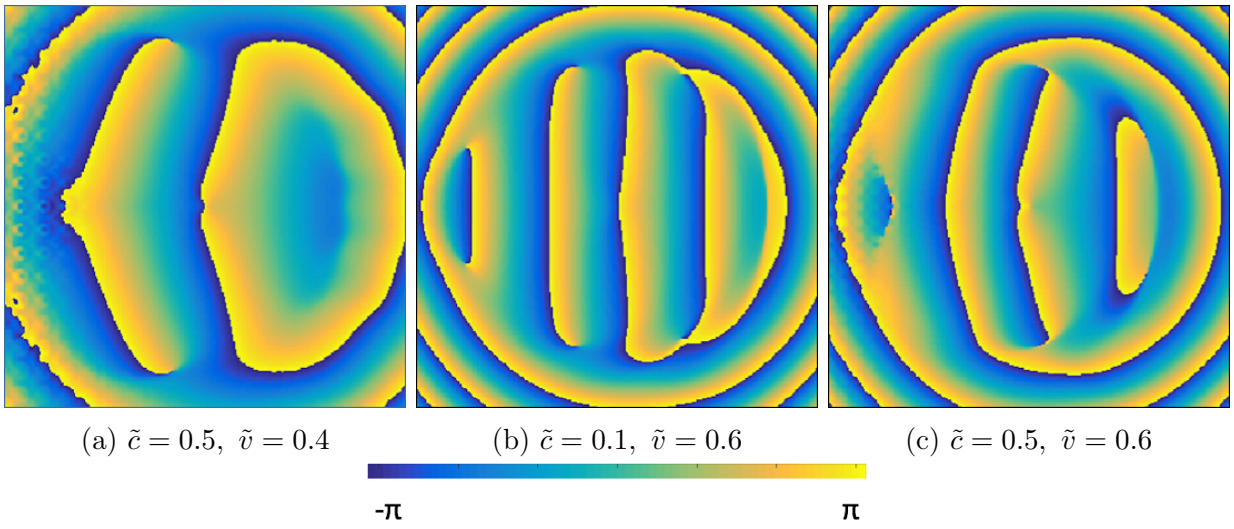

(a) $\tilde{c} = 0.5,\ \tilde{v} = 0.4$ (b) $\tilde{c} = 0.1,\ \tilde{v} = 0.6$ (c) $\tilde{c} = 0.5,\ \tilde{v} = 0.6$

Figure 4.3: Phase plots for figures 4.1 (e) ((a) here), (g) ((b) here) and (h) ((c) here). The phase and corresponding density plots have the same scale (in size).

4.2 Gaussian Starting Inside the Droplet

When the Gaussian starts inside the droplet, see figure 1.1, one can compare the results with the classical fluid and trapped BEC cases. However, for the two broader Gaussians, the obstacle-fluid ratio might still be too big. One can also compare to when the gaussian started outside the droplet. Further, Landau's criterion is relevant since the Gaussian starts inside the droplet and far away from its surface, where the density is relatively uniform.

Figure 4.4 shows the density distribution of the droplet for different Gaussian widths and droplet velocities at time t_2' in figure 1.1. In all the plots of figure 4.4, one can see that the density distribution within the droplet is different from that in figure 4.2. Note that I am not referring to the "polka dot pattern", this will be discussed further down. This suggests that Landau's criterion has been broken and that the droplet no longer fully behaves like a superfluid, assuming the surface of the droplet is not impacting it. However, compared to when the gaussian started outside the droplet, the droplet has recombined behind the Gaussian in all plots. This suggest that the piercing of the droplet by the Gaussian is responsible for this deformation in that case.

Compared to the classical fluid and trapped BEC cases, none of the plots in the right column of figure 4.4 show the existence of vortex streets. Neither of the corresponding phase plots show vortices attached to the Gaussian either. The phase plot of figure 4.4 (g) is shown as an example in figure 4.5 (a).

In none of the other cases in figure 4.4, attached vortices could be found in the corresponding phase plots. The phase plots of figure 4.4 (h) and (i) are shown in figure 4.5 (b) and (c) as examples. There is also no sign of vortex streets in the density plots.

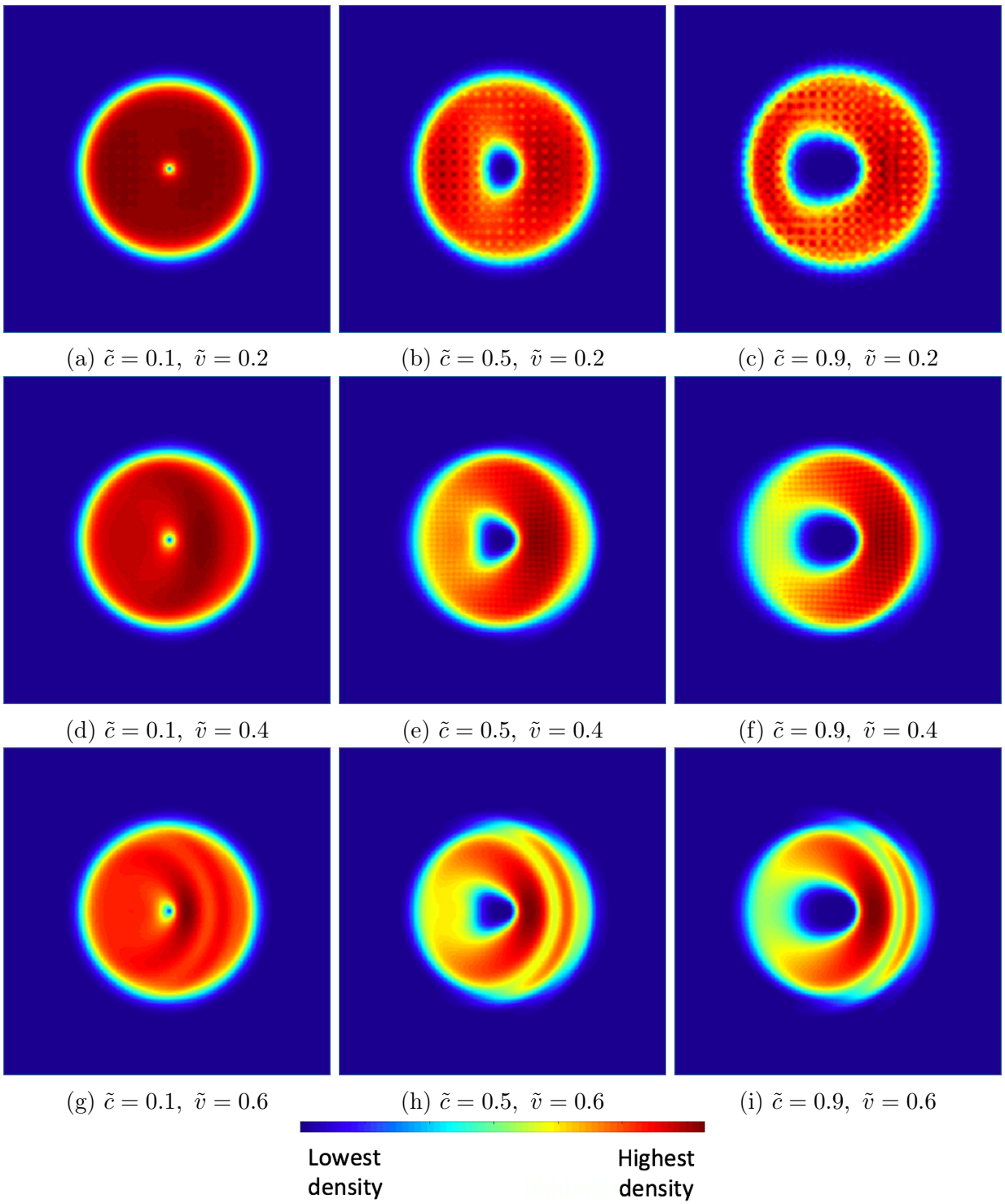

(a) $\tilde{c} = 0.1,\ \tilde{v} = 0.2$ (b) $\tilde{c} = 0.5,\ \tilde{v} = 0.2$ (c) $\tilde{c} = 0.9,\ \tilde{v} = 0.2$

(d) $\tilde{c} = 0.1,\ \tilde{v} = 0.4$ (e) $\tilde{c} = 0.5,\ \tilde{v} = 0.4$ (f) $\tilde{c} = 0.9,\ \tilde{v} = 0.4$

(g) $\tilde{c} = 0.1,\ \tilde{v} = 0.6$ (h) $\tilde{c} = 0.5,\ \tilde{v} = 0.6$ (i) $\tilde{c} = 0.9,\ \tilde{v} = 0.6$

Figure 4.4: Density distribution of the dilute BEC droplet when the Gaussian started inside the droplet, for different Gaussian sizes and droplet velocities, at time t_2' in figure 1.1. The dimensionless Gaussian sizes $\tilde{c}$ and velocities $\tilde{v}$ are given in the figure. Note that for example dark red is the highest density in each plot, but that it might not correspond to the same density value in all of them. The Gaussians are not plotted in the figure, but are in the middle of each plot. They can in part indirectly be seen by the interaction with the droplet.

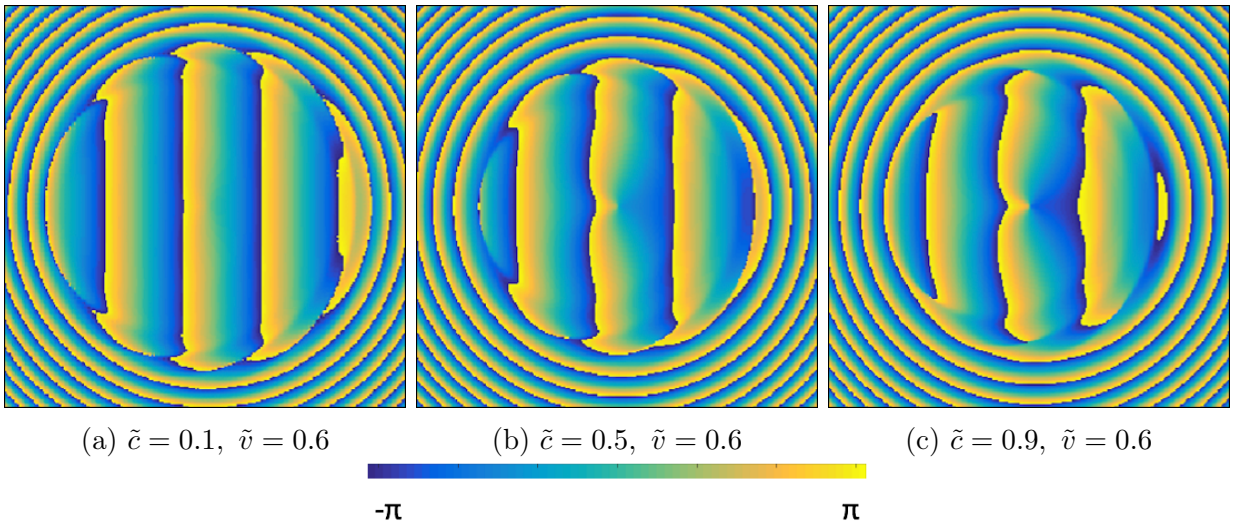

(a) $\tilde{c} = 0.1,\ \tilde{v} = 0.6$ (b) $\tilde{c} = 0.5,\ \tilde{v} = 0.6$ (c) $\tilde{c} = 0.9,\ \tilde{v} = 0.6$

Figure 4.5: Phase plots for figures 4.4 (g) ((a) here), (h) ((b) here) and (i) ((c) here). The phase and corresponding density plots have the same scale (in size).

Regarding the "polka dot pattern" seen in several pictures of figure 4.4, it could be excitations that arise from introducing the gaussian infinitely fast at $t = 0$ s inside the droplet. This would help to break Landau's criterion faster. Therefore, the ground state of the droplet should be formed around the Gaussian in the future instead. More simulations would have to be made to see if there is a laminar flow regime.

However, it might that Landau's criterion has not been broken in any of the plots in figure 4.4. The drag force might again be due to quantum fluctuations [29].

Again, it is hard to explain why the flow pattern looks the way they do (apart from the droplet not behaving fully like a superfluid). However, an intuitive comparison for the patterns in the bottom row of figure 4.4 is having a piece of fabric lying flat on a table, taking it by the end and dragging it towards a cylindrical object on the table. Then the fabric will wrap around the cylinder and form these crests (or high density regions).

Chapter 5

Conclusion and Outlook

In conclusion, for none of the Gaussian widths and droplet velocities tested, a laminar flow regime, attached vortices to the back of the Gaussian or a vortex street was/were found. This was when starting with the Gaussian outside the droplet as well as inside, see figure 1.1. It appeared that in all the cases the droplet did not fully behave like a superfluid. It also seems as large deformation of the droplet only occurs in the case when a broad Gaussian starts outside the droplet. No similarities to the classical fluid flowing past a cylinder or trapped BEC cases with a Gaussian could be found.

Potential future research could include many things. First of all, in the case where the Gaussian starts inside the droplet, the droplet ground state should be formed around the Gaussian if possible. This would be more physically accurate than inserting the Gaussian infinitely fast at $t = 0$. Secondly, the droplet could be studied after it passed the Gaussian. Some simulations were done on this while working on this thesis. In some cases, the droplet passes through and stayed together, in other cases, it broke and sometimes it bounced back when hitting the Gaussian initially. In other cases, it even seemed to almost get stuck on the Gaussian. One could also study the droplet when the Gaussian just pierces or leaves the droplet. Further, one could use velocity plots to better study the flow patterns of the droplet. This was tried in this thesis, but some technical issues arose. One could also include three-body losses. Finally, the collision of a dilute BEC droplet with a double slit could also be studied. The double slit experiment is a very famous experiment in quantum mechanics and it would be very interesting to try with a dilute BEC droplet.

Bibliography

[1] G. Ohlén, *Phenomena of the Quantum World, Theory and Concepts* (Department of Physics, Lund University, 2016).

[2] C. J. Pethick and H. Smith, *Bose-Einstein Condensation in Dilute Gases* (Cambridge University Press, Cambridge, 2002).

[3] L. Pitaevskii and S. Stringari, *Bose-Einstein Condensation* (Clarendon Press, Oxford, 2003).

[4] S. Bargi, Ph.D. thesis, Lund University, 2010.

[5] E. K. U. Gross, E. Runge and O. Heinonen, *Many-Particle Theory* (Adam Hilger, Bristol, Philadelphia and New York, 1991).

[6] P. Stürmer, M.Sc. thesis, Lund University, 2019.

[7] M. Aichinger, S. A. Chin and E. Krotscheck, Comput. Phys. Commun. **171**, 3, 197 (2015).

[8] D. S. Petrov, Phys. Rev. Lett. **115**, 155302 (2015).

[9] I. Ferrier-Barbut, Phys. Today **72**, 4, 46 (2019).

[10] C. R. Cabrera *et al.*, Science **359**, 6373, 301 (2018).

[11] I. Ferrier-Barbut *et al.*, Phys. Rev. Lett. **116**, 215301 (2016).

[12] H. Kadau *et al.*, Nature **530**, 194 (2015).

[13] T. D. Lee, K. Huang and C-N. Yang, Phys. Rev. **106**, 1135 (1957).

[14] What is a superfluid?, Physics World, https://physicsworld.com/a/what-is-a-superfluid/ (2016) (Accessed 10-05-2020).

[15] G. W. Stagg *et al.*, J. Phys.: Conf. Ser. **594**, 012044 (2015).

[16] D. J. Tritton, *Physical Fluid Dynamics* (Clarendon Press, Oxford, 1988).

[17] D. J. Griffiths, *Introduction to Quantum Mechanics* (Prentice Hall, New Jersey, 1995).

[18] D. S. Petrov and G. E. Astrakharchik, Phys. Rev. Lett. **117**, 100401 (2016).

[19] G. Semeghini *et al.*, Phys. Rev. Lett. **120**, 235301 (2018).

[20] Viscosity, Encyclopaedia Britannica, https://www.britannica.com/science/viscosity (Accessed 10-05-2020).

[21] D. A. Butts and D. S. Rokhsar, Nature **397**, 327 EP (1999).

[22] P. C. Haljan *et al.*, Phys. Rev. Lett. 87, 210403 (2001).

[23] M. Nilsson Tengstrand *et al.*, Phys. Rev. Lett. **123**, 160405 (2019).

[24] K. Sasaki, N. Suzuki and H. Saito, Phys. Rev. Lett. **104**, 150404 (2010).

[25] P. Bader, S. Blanes and F. Casas, J. Chem. Phys. **139**, 12, 124117 (2013).

[26] R. I. McLachlan and G. R. W. Quispel, Acta Numerica **11**, 341 (2002).

[27] Gaussian Function, Science Direct, https://www.sciencedirect.com/topics/engineering/gaussian-function (Accessed 10-05-2020).

[28] M. Nilsson Tengstrand *et al.*, Phys. Rev. Lett. 123, 160405 (2019) (to be published).

[29] D. C. Roberts and Y. Pomeau, Phys. Rev. Lett. **95**, 145303 (2005).